Editors' Suggestion | Featured in Physics

Candidate for Laser Cooling of a Negative Ion: High-Resolution Photoelectron Imaging of Th^-

Rulin Tang,[1,§] Ran Si,[2,3,§] Zejie Fei,[4] Xiaoxi Fu,[1] Yuzhu Lu,[1] Tomas Brage,[2,3] Hongtao Liu,[4,*] Chongyang Chen,[3,†] and Chuangang Ning[1,5,‡]

[1]*Department of Physics, State Key Laboratory of Low-Dimensional Quantum Physics, Tsinghua University, Beijing 100084, China*

[2]*Lund University, Department of Physics, P.O. Box 118, 221 00 Lund, Sweden*

[3]*Shanghai EBIT Lab, Key Laboratory of Nuclear Physics and Ion-beam Application (MOE), Institute of Modern Physics, Department of Nuclear Science and Technology, Fudan University, Shanghai 200433, China*

[4]*Key Laboratory of Interfacial Physics and Technology, Shanghai Institute of Applied Physics, Chinese Academy of Sciences, Shanghai 201800, China*

[5]*Collaborative Innovation Center of Quantum Matter, Beijing 100084, China*

(Received 9 June 2019; revised manuscript received 14 August 2019; published 12 November 2019)

Laser cooling is a well-established technique for the creation of ensembles of ultracold neutral atoms or positive ions. This ability has opened many exciting new research fields over the past 40 years. However, no negatively charged ions have been directly laser cooled because a cycling transition is very rare in atomic anions. Efforts of more than a decade currently have La^- as the most promising candidate. We report on experimental and theoretical studies supporting Th^- as a new promising candidate for laser cooling. The measured and calculated electron affinities of Th are, respectively, 4901.35(48) cm^{-1} and 4832 cm^{-1}, or 0.607 690(60) and 0.599 eV, almost a factor of 2 larger than the previous theoretical value of 0.368 eV. The ground state of Th^- is determined to be $6d^37s^2\,{}^4F^e_{3/2}$ rather than $6d^27s^27p\,{}^4G^o_{5/2}$. The consequence of this is that there are several strong electric dipole transitions between the bound levels arising from configurations $6d^37s^2$ and $6d^27s^27p$ in Th^-. The potential laser-cooling transition is ${}^2S^o_{1/2} \leftrightarrow {}^4F^e_{3/2}$ with a wavelength of 2.6 μm. The zero nuclear spin and hence lack of hyperfine structure in Th^- reduces the potential complications in laser cooling as encountered in La^-, making Th^- a new and exciting candidate for laser cooling.

DOI: 10.1103/PhysRevLett.123.203002

In 1978, several seminal experiments demonstrated that atoms and cations can be slowed down by using the radiation pressure of a laser beam tuned to a resonance [1–3]. Over the past 40 years, laser cooling of neutral atoms and cations has revolutionized the ability to control and manipulate atoms and ions to an ultracold regime, which has opened many exciting new research fields, such as Bose-Einstein condensation, precision spectroscopy, and tests of fundamental symmetries [4,5]. However, laser cooling of anions has not yet been achieved due to the lack of suitable electric dipole ($E1$) transition. The binding of the extra electron with the neutral core in an anion is dominated by polarization and correlation effects [6]. Therefore, in contrast to the infinite number of bound states for neutral atoms and cations, anions usually have only one bound state. A few atomic anions have bound excited states, but it is even rarer that they possess bound states of opposite parity. Electric dipole transitions between bound states have previously been observed only in three atomic anions: Os^- [7–11], Ce^- [12,13], and La^- [11,14–16]. The former two, Os^- and Ce^-, are not ideal for laser cooling due to the fact that the transitions are slow and the upper states decay to multiple metastable lower states, requiring repumping out of dark states. The most promising known candidate for laser cooling is therefore, so far, La^- [16]. (In addition, among molecular anions, C_2^- is also a potential candidate [17].) In principle, once one kind of negative ion is laser cooled, other negative-ion species can be cooled sympathetically by confining them simultaneously in a trap. A particularly exciting application is to sympathetically cool antiprotons in the production of ultracold antihydrogen for a test of the symmetry between matter and antimatter and the gravitational acceleration of antimatter [18–21]. To achieve antihydrogen temperatures lower than can be reached by the mixing of antiprotons and positrons in a nested Penning-Malmberg trap [22], the charge exchange reaction between positronium and cold antiprotons may be used [23]. Because of the large antiproton-positron mass ratio, the final antihydrogen temperature is near the initial antiproton temperature. Furthermore, laser cooling of anions could open previously inaccessible research fields in which ultracold negative ions

are required, such as cold chemistry or cold plasmas [24,25]. Obviously, the experimental search for the atomic anion with a bound-bound $E1$ transition is the first important step for laser cooling of negative ions.

Besides the predictions for atomic anions with bound states of opposite parity in the lanthanide group, e.g., La^- and Ce^-, O'Malley and Beck [26] also predicted that some atomic anions in the actinide group, e.g., Th^- and U^-, have such excited states. However, the electron affinity values of Th and U were estimated to be only about 0.3 eV, which makes them unsuitable candidates for laser cooling. As an example, the binding energy (BE) of the odd ground state $6d^27s^27p\,{}^4G^o_{5/2}$ of Th^- was predicted to be 0.368 eV, while the BE was predicted to be 0.304 eV for the lowest even state $6d^37s^2\,{}^4F^e_{3/2}$. The lower the binding energy is, the slower the cycling transition will be because the spontaneous decay rate is proportional to ΔE^3 for dipole transitions, where ΔE is the transition energy.

Here we report on a measurement of the electron affinity value of a Th atom of about 0.6 eV, which is almost twice the earlier estimate. We also present improved calculations, which are in agreement with this observation, and predict the ground state of Th^- to be $6d^37s^2\,{}^4F^e_{3/2}$ rather than $6d^27s^27p\,{}^4G^o_{5/2}$. By performing large-scale multiconfiguration Dirac-Hartree-Fock (MCDHF) calculations, we show that the transition $6d^27s^27p\ {}^2S^o_{1/2} \leftrightarrow 6d^37s^2\,{}^4F^e_{3/2}$ (with $\lambda \approx 2.6\ \mu$m) in this anion is an ideal cycling transition for laser cooling, which makes Th^- a promising candidate for laser cooling of a negative ion. Furthermore, one advantage of Th^-, compared to La^-, is the zero nuclear spin of its only stable isotope, ^{232}Th. In comparison, the La^- stable isotope ^{139}La has a nuclear spin of $7/2$ resulting in a complex pattern of nine hyperfine components in the candidate transition ($\lambda \approx 3.1\ \mu$m) between the ground state $^3F^e_2$ and the excited state $^3D^o_1$ [16], in turn leading to a complicated repumping laser system.

To the best of our knowledge, no experimental electron affinity value of Th has yet been reported. In this Letter, we present the high-resolution binding energy spectrum of Th^- from our newly built photoelectron-imaging spectrometer. Its main features are the high energy resolution of the slow-electron velocity-map imaging technique [27,28], typically a few cm^{-1} near the photodetachment threshold, and the cold ion trap [29,30] with a controlled temperature in the range 5–300 K. With this apparatus, we have recently significantly improved the accuracies in electron affinity (EA) measurements for several transition metal elements [31–35]. The detailed description of the spectrometer can be found elsewhere [36], but, briefly, it consists of a laser ablation ion source, a cold octupole radio-frequency (rf) ion trap, a time-of-flight mass spectrometer, and a photoelectron velocity-map imaging system. Th^- anions are produced via the pulsed Nd:Y-Al-garnet laser ablation of a thorium metal disk. The hot anions lose their kinetic energy through collisions with a burst of gas, which is delivered into the ion trap via a pulsed valve. The anions are then accumulated and cooled via buffer gas cooling in the ion trap for 45 ms. The buffer gas is evacuated after cooling. The stored anions are ejected out via pulsed potentials on the end caps of the ion trap, and analyzed via time-of-flight mass spectrometry. Th^- anions are selected via a mass gate, then photodetached by a tunable dye laser in the interaction region of the velocity-map imaging system. The hitting positions of outgoing photoelectrons are recorded by a microchannel-plate enhanced CCD camera in the event-counting mode. The three-dimensional photoelectron distributions are reconstructed from the projected two-dimensional image via the method of maximum-entropy reconstruction of velocity maps [37]. The photoelectrons with the same velocity form a spherical shell, where the radius of the shell r is proportional to their velocity, leaving their kinetic energy E_k proportional to r^2, i.e., $E_k = \alpha r^2$. The coefficient α can be determined by varying the photon energy $h\nu$. In addition, the photoelectron angular distribution is also simultaneously measured. The spectrometer runs at a 20-Hz repetition rate.

Figure 1 shows the photoelectron image at a photon energy of $\nu/c = 15\,397\ cm^{-1}$, and the combined binding energy spectra with a series of photon energies. In order to distinguish transitions from different initial states, different buffer gases of the ion trap were used. A mixture of 20% H_2 and 80% He gas is usually more effectively deexciting

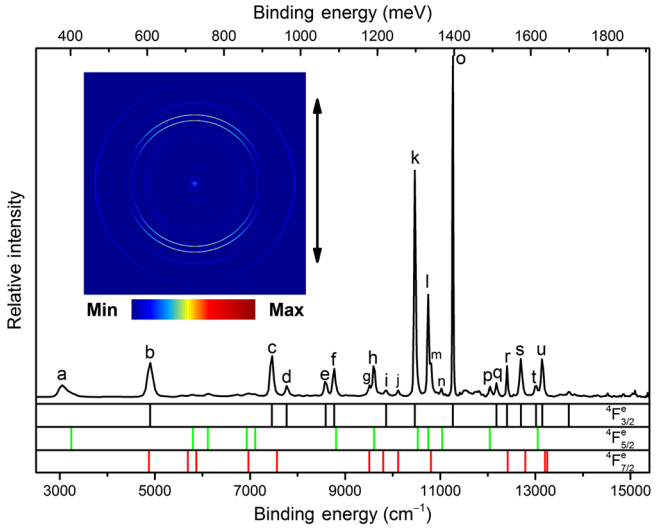

FIG 1. High-resolution photoelectron spectra of Th^-. A series of vertical sticks represent the relative energy levels of the neutral Th atom. The colors of vertical sticks indicate three different bound states of Th^-: black for transitions from the ground state $^4F^e_{3/2}$ of Th^-, green for the first excited state, $^4F^e_{5/2}$, and red for the second excited state, $^4F^e_{7/2}$. The measured binding energies of all peaks are listed in the Supplemental Material [39]. (Inset) The photoelectron image at $\nu/c = 15\,397\ cm^{-1}$. The double arrow indicates the laser polarization. See the text for details.

metastable states of atomic anions than pure He gas. Thus the intensity of the peak corresponding to photodetachment from a common initial state shows the same dependence on the buffer gas (see the Supplemental Material [38]), which supports their identification. Moreover, the energy levels of the neutral Th atom are known to a high accuracy [39,40], giving a "fingerprint" in support of the state assignment. In Fig. 1, the black bars below the energy spectrum indicate the positions of peaks from the ground state of Th^-. The relative positions of the bars are locked according to the energy levels of Th, as described above. Similarly, the green bars indicate the first observed excited states of Th^-, and the red bars the second observed excited states. In combination with the large-scale MCDHF calculations discussed below and the selection rules of photodetachment [41], the ground state of Th^- is assigned as $6d^37s^2\,{}^4F^e_{3/2}$. The two observed excited states are $6d^37s^2\,{}^4F^e_{5/2}$ and ${}^4F^e_{7/2}$, respectively. The lifetime of the two excited states should be comparable to or much longer than 45 ms since they were observed after Th^- anions were stored in the trap for 45 ms. The detailed assignments of the peaks are given in Fig. 2 and the Supplemental Material [38]. Since the photodetachment energy from the anionic ground state $Th^-(6d^37s^2\,{}^4F^e_{3/2})$ to the neutral ground state $Th(6d^27s^2\,{}^3F_2)$ is out of tuning range of our dye laser, the strong peak labeled o $(6d^37s^2\,{}^4F^e_{3/2} \rightarrow 6d^37s\,{}^5F_2)$ is selected as the target channel for the present EA measurement. The preliminary measurement of the BE of peak o can help us to narrow down the range for performing a series of low-kinetic-energy photoelectron measurements to achieve a highly accurate EA value.

To accurately determine BE of peak o, the photon energy ν/c is varied from 11 295 to 11 438 cm^{-1}, which is slightly above the photodetachment threshold of this peak. In Fig. 3, the linear (since $h\nu = \mathrm{BE} + \alpha r^2$) experimental data plot of ν/c versus r^2 gives the BE value as the intercept of the fitted line with the ν/c axes. The coefficient α is also determined during this procedure. The resulting BE value is 11 263.75(48) cm^{-1}. Since the final state of photodetachment channel o, $Th[6d^37s\,{}^5F_2]$, is 6362.396 cm^{-1} above the ground state of Th [39,40], the EA of Th is determined to be 4901.35(48) cm^{-1} or 0.607 690(60) eV (using 1 eV = 8065.543 937 cm^{-1}, as recommended by 2018 CODATA [42]). This is significantly different than the previous prediction by O'Malley and Beck [26] and opens up for this anion to be used for laser cooling. For the theoretical part of this work, we used the MCDHF method [43] implemented in the GRASP2K package [44]. The MCDHF method is based on a representation of the atomic system by atomic state functions expanded in a basis of configuration state functions (CSFs). The list of CSFs is generated by using an active space approach [45]. Typically, one defines a multireference (MR) set with the most important CSFs, then allows for, e.g., single and double (SD) substitutions to an active set of orbitals.

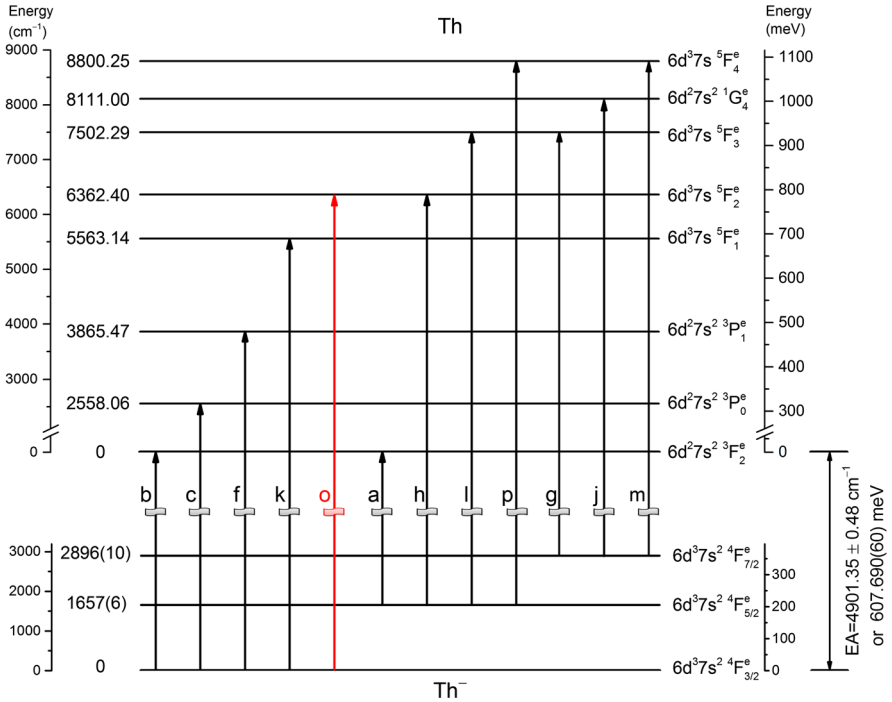

FIG. 2. Partial energy levels of Th and Th^- related to the present measurement. The labels of each photodetachment channel are the indexes of the observed peaks in Fig. 1. The photodetachment channel o, $Th^-(^4F^e_{3/2}) \rightarrow Th\,(^5F_2)$, is used for the electron affinity measurement.

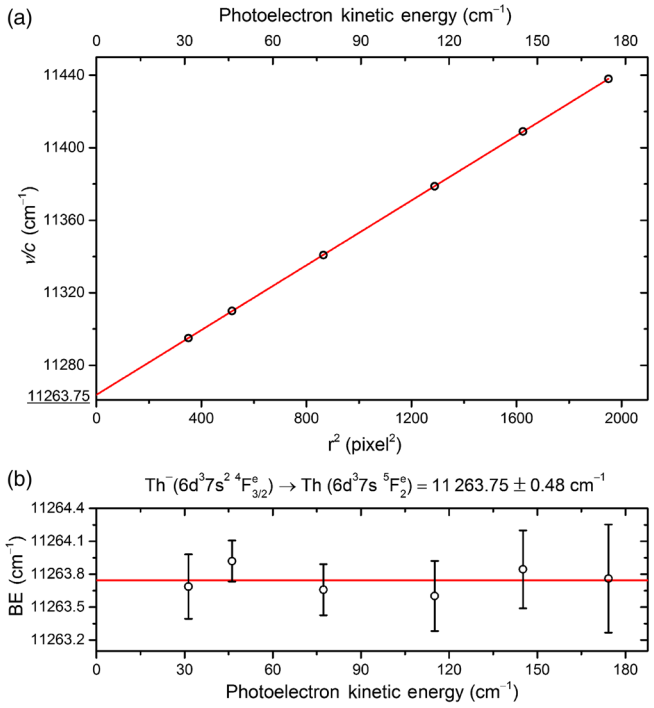

FIG. 3. (a) The photon energy ν/c versus the squared radius r^2 for the photodetachment channel o. The solid line is the linear least squares fitting. The intercept 11 263.75 cm^{-1} is the binding energy of transition o. (b) The uncertainty of the binding energy of Th$^-$($^4F^e_{3/2}$) → Th($^5F_2$) versus the kinetic energy of the photoelectrons.

The radial parts of the Dirac orbitals and the expansion coefficients of a number of targeted states were obtained iteratively in the relativistic self-consistent field procedure. The Breit interaction in its low-frequency limit and QED effects (self-energy and vacuum polarization) are added in a subsequent relativistic configuration interaction calculation [46], where only the expansion coefficients were determined by diagonalizing the Hamiltonian matrix.

To explore the important CSFs for the ground states of both the neutral atom and the negative ion, we start with a single reference calculation. In this work, the CSF list is generated by allowing SD excitations from the $6p$, $6d$, and $7s$ subshells in the $6d^27s^2$ configuration of Th, as well as the $6d^37s^2$ and $6d^27s^27p$ configurations of Th$^-$ to an active set of orbitals with $n \le 9$, $l \le 4$. The CSFs with wave function compositions above 1% come from configurations $6d^27s^2$, $6d^37s$, and $6d^4$ for the ground state $6d^27s^2\,^3F_2$ in Th, from $6d^37s^2$, $6d^27s7p^2$, and $6d^37p^2$ for the lowest state $6d^37s^2\,^4F^e_{3/2}$ in Th$^-$ with even parity, and from $6d^27s^27p$, $6d^37s7p$, and $6d^47p$ for the lowest state $6d^27s^27p\,^4G^o_{5/2}$ in Th$^-$ with odd parity. They are defined as the MR configurations for the different states in the final structure calculations for Th and Th$^-$. Furthermore, by allowing the $6d$, $7s$, and $7p$ valence electron together with the $6p$ core electron in these MR configurations to be SD excited to active sets with $n \le 11$, $l \le 4$, we include the valence-valence correlation effect, and the core-valence and core-core correlation effects due to the $6p$ electrons.

TABLE I. Measured and calculated excitation energies of Th$^-$ states, and the electron affinity of Th.

	Measured		Calculated	
State	cm^{-1}	meV	cm^{-1}	meV
$6d^37s^2\,^4F^e_{3/2}$			0	0
$6d^27s^27p\,^4G^o_{5/2}$			401	50
$6d^37s^2\,^4F_{5/2}$	1657(6)	205.4(7)	1377	171
$6d^37s^2\,^4F_{7/2}$	2896(10)	359.1(12)	2642	328
$6d^27s^27p\,^4F^o_{3/2}$			3033	376
$6d^37s^2\,^4F_{9/2}$			3637	451
$6d^27s^27p\,^2S^o_{1/2}$			3904	484
$6d^27s^27p\,^4F^o_{7/2}$			3974	493
$6d^27s^27p\,^4F^o_{5/2}$			3992	495
Electron affinity of Th	4901.35(48)	607.690(60)	4832	599

Following the method described in our previous paper [47], the calculated electron affinity of Th is 4832 cm^{-1}, or 0.599 eV, and the ground state of Th$^-$ is determined to be $6d^37s^2\,^4F^e_{3/2}$ rather than $6d^27s^27p\,^4G^o_{5/2}$. The odd anion state is above the even one by 401 cm^{-1} (0.050 eV), as seen in Table I, in which the calculated energies for the lowest-lying levels of Th$^-$ are listed. This is in contrast to the earlier prediction of the ground state of Th$^-$ as $6d^27s^27p\,^4G^o_{5/2}$ [26,48]. In these earlier calculations, the core-valence and

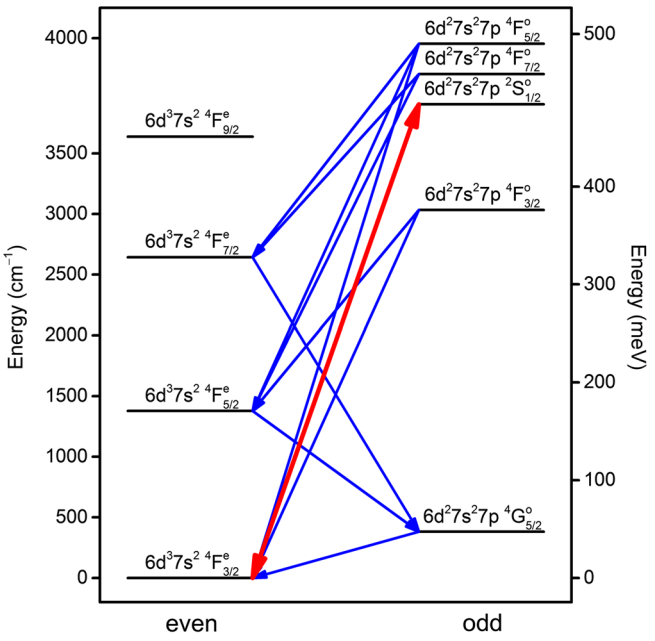

FIG. 4. The partial energy level diagram of Th$^-$. The arrows indicated the electric dipole transition between states of even parity ($6d^37s^2$) and odd parity ($6d^27s^27p$). The red bold arrow indicates the potential laser-cooling transition $^2S^o_{1/2} \leftrightarrow {}^4F^e_{3/2}$.

TABLE II. Calculated electric dipole transition energies, transition rates A, and lifetimes τ. Numbers in brackets represent powers of 10.

Upper level	Lower level	Energy cm^{-1}	Energy meV	A (s^{-1})	τ
$6d^27s^27p\ {}^4G^o_{5/2}$	$6d^37s^2\ {}^4F^e_{3/2}$	401	50	1.95[+1]	51.3 ms
$6d^37s^2\ {}^4F^e_{5/2}$	$6d^27s^27p\ {}^4G^o_{5/2}$	976	121	2.08[+0]	0.458 s
$6d^37s^2\ {}^4F^e_{7/2}$	$6d^27s^27p\ {}^4G^0_{5/2}$	2241	278	1.24[+2]	8.08 ms
$6d^27s^27p\ {}^4F^o_{3/2}$	$6d^37s^2\ {}^4F^e_{3/2}$	3033	376	6.26[+4]	15.9 μs
	$6d^37s^2\ {}^4F_{5/2}$	1656	205	2.01[+2]	
$6d^27s^27p\ {}^2S^o_{1/2}$	$6d^37s^2\ {}^4F^e_{3/2}$	3904	484	1.17[+4]	85.5 μs
$6d^27s^27p\ {}^4F^o_{7/2}$	$6d^37s^2\ {}^4F_{5/2}$	2597	322	6.86[+3]	138 μs
	$6d^37s^2\ {}^4F_{7/2}$	1332	165	4.01[+2]	
$6d^27s^27p\ {}^4F^o_{5/2}$	$6d^37s^2\ {}^4F^e_{3/2}$	3992	495	1.40[+4]	42.4 μs
	$6d^37s^2\ {}^4F_{5/2}$	2615	324	9.57[+3]	
	$6d^37s^2\ {}^4F_{7/2}$	1350	167	5.82[+1]	

core-core correlation effects with the $6p$ electrons were not included.

Decay branching fractions and transition rates of the bound levels of anions are two key aspects of laser cooling. Here the $E1$ transition rates are calculated within length (Babushkin) form [49] by using the biorthonormal transformation [50]. Figure 4 and Table II show the $E1$ transitions in Th^-. The lifetime of ${}^4G^o_{5/2}$ is predicted to be 51.3 ms. In principle, ${}^4G^o_{5/2}$ should be observed in the present experiment. However, no peak can be assigned to the transition related to ${}^4G^o_{5/2}$. It is either due to a much shorter lifetime than the predicted one or due to a very weak photodetachment channel.

To conclude, the ground state of Th^- was assigned as the even $6d^37s^2\ {}^4F^e_{3/2}$ state with a binding energy 0.607 690(60) eV. The potential candidate for laser cooling is the transition ${}^2S^o_{1/2} \leftrightarrow {}^4F^e_{3/2}$. At first glance, it could be argued that our new transition is spin forbidden, but due to severe state mixing, caused by the breakdown of the LS-coupling scheme in Th-, it is not as relevant. The main composition of ${}^2S^o_{1/2}$ is $26\%{}^2S^o_{1/2} + 18\%{}^4P^o_{1/2} + 11\%{}^4D^o_{1/2}$. All possible $E1$ transitions illustrated in Fig. 4 have considered this state mixing. The transition energy is calculated to be 3904 cm^{-1} ($\lambda \approx 2.6\ \mu$m), and the transition rate is 1.17×10^4 s^{-1}. The minimum temperature T_D achievable with Doppler cooling is $\sim$0.04 μK. Considering the rf heating effect, the temperature of Th^- anions achievable with buffer cooling is $\sim$10 K with buffer gas He at 5 K. For one-dimensional cooling of an ensemble of Th^- anions from 10 K to T_D, it will require the absorption and emission of 2.7×10^4 photons and hence take 2.6 s if in saturation.

This work is supported by the National Natural Science Foundation of China (NSFC) (Grants No. 91736102, No. 11974199, No. 21573273, and No. 11674066), the National Key R&D Program of China (Grant No. 2018YFA0306504), and the Strategic Priority Research Program of the Chinese Academy of Sciences (Grant No. XDA02020000). R. S. and T. B. would like to acknowledge the support of the Swedish Research Council (VR) under Contract No. 2015-04842. H. L. would like to acknowledge the support of the Hundred Talents Program (CAS).

*liuhongtao@sinap.ac.cn
†chychen@fudan.edu.cn
‡ningcg@tsinghua.edu.cn
§These authors contributed equally to this work.

[1] A. Ashkin Phys. Rev. Lett. **40**, 729 (1978).
[2] D. J. Wineland, R. E. Drullinger, and F. L. Walls, Phys. Rev. Lett. **40**, 1639 (1978).
[3] W. Neuhauser, M. Hohenstatt, P. Toschek, and H. Dehmelt, Phys. Rev. Lett. **41**, 233 (1978).
[4] C. E. Wieman, D. E. Pritchard, and D. J. Wineland, Rev. Mod. Phys. **71**, S253 (1999).
[5] A. D. Cronin, J. Schmiedmayer, and D. E. Pritchard, Rev. Mod. Phys. **81**, 1051 (2009).
[6] T. Andersen Phys. Rep. **394**, 157 (2004).
[7] R. C. Bilodeau and H. K. Haugen, Phys. Rev. Lett. **85**, 534 (2000).
[8] A. Kellerbauer and J. Walz, New J. Phys. **8**, 45 (2006).
[9] U. Warring, M. Amoretti, C. Canali, A. Fischer, R. Heyne, J. O. Meier, C. Morhard, and A. Kellerbauer, Phys. Rev. Lett. **102**, 043001 (2009).
[10] A. Fischer, C. Canali, U. Warring, A. Kellerbauer, and S. Fritzsche, Phys. Rev. Lett. **104**, 073004 (2010).
[11] L. Pan and D. R. Beck, Phys. Rev. A **82**, 014501 (2010).
[12] C. W. Walter, N. D. Gibson, C. M. Janczak, K. A. Starr, A. P. Snedden, R. L. Field III, and P. Andersson, Phys. Rev. A **76**, 052702 (2007).
[13] C. W. Walter, N. D. Gibson, Y. G. Li, D. J. Matyas, R. M. Alton, S. E. Lou, R. L. Field, D. Hanstorp, L. Pan, and D. R. Beck, Phys. Rev. A **84**, 032514 (2011).
[14] C. W. Walter, N. D. Gibson, D. J. Matyas, C. Crocker, K. A. Dungan, B. R. Matola, and J. Rohlen, Phys. Rev. Lett. **113**, 063001 (2014).
[15] E. Jordan, G. Cerchiari, S. Fritzsche, and A. Kellerbauer, Phys. Rev. Lett. **115**, 113001 (2015).
[16] G. Cerchiari, A. Kellerbauer, M. S. Safronova, U. I. Safronova, and P. Yzombard, Phys. Rev. Lett. **120**, 133205 (2018).
[17] P. Yzombard, M. Hamamda, S. Gerber, M. Doser, and D. Comparat, Phys. Rev. Lett. **114**, 213001 (2015).
[18] M. Amoretti *et al.*, Nature (London) **419**, 456 (2002).
[19] M. Ahmadi *et al.*, Nature (London) **541**, 506 (2017).
[20] S. Gerber, J. Fesel, M. Doser, and D. Comparat, New J. Phys. **20**, 023024 (2018).
[21] A. Kellerbauer *et al.*, Nucl. Instrum. Methods Phys. Res., Sect. B **266**, 351 (2008).
[22] M. Ahmadi *et al.*, Nat. Commun. **8**, 681 (2017).
[23] M. Doser *et al.* (AEGIS Collaboration), Classical Quantum Gravity **29**, 184009 (2012).

[24] D. S. Jin and J. Ye, Chem. Rev. **112**, 4801 (2012).
[25] T. K. Langin, G. M. Gorman, and T. C. Killian, Science **363**, 61 (2019).
[26] S. M. O'Malley and D. R. Beck, Phys. Rev. A **80**, 032514 (2009).
[27] A. Osterwalder, M. J. Nee, J. Zhou, and D. M. Neumark, J. Chem. Phys. **121**, 6317 (2004).
[28] I. León, Z. Yang, H. T. Liu, and L. S. Wang, Rev. Sci. Instrum. **85**, 083106 (2014).
[29] C. Hock, J. B. Kim, M. L. Weichman, T. I. Yacovitch, and D. M. Neumark, J. Chem. Phys. **137**, 244201 (2012).
[30] X. B. Wang and L. S. Wang, Rev. Sci. Instrum. **79**, 073108 (2008).
[31] Z. H. Luo, X. L. Chen, J. M. Li, and C. G. Ning, Phys. Rev. A **93**, 020501(R) (2016).
[32] X. L. Chen and C. G. Ning, Phys. Rev. A **93**, 052508 (2016).
[33] X. L. Chen and C. G. Ning, J. Phys. Chem. Lett. **8**, 2735 (2017).
[34] R. L. Tang, X. L. Chen, X. X. Fu, H. Wang, and C. G. Ning, Phys. Rev. A **98**, 020501(R) (2018).
[35] Y. Lu, R. L. Tang, X. X. Fu, and C. G. Ning, Phys. Rev. A **99**, 062507 (2019).
[36] R. L. Tang, X. X. Fu, and C. G. Ning, J. Chem. Phys. **149**, 134304 (2018).
[37] B. Dick Phys. Chem. Chem. Phys. **16**, 570 (2014).
[38] See Supplemental Material at http://link.aps.org/supplemental/10.1103/PhysRevLett.123.203002 for a comparison of photoelectron spectra with different trapping times and an assignment of all observed peaks.
[39] R. Zalubas J. Res. Natl. Bur. Stand., Sect. A **63**, 275 (1959).
[40] S. L. Redman, G. Nave, and C. J. Sansonetti, Astrophys. J. Suppl. Ser. **211**, 4 (2014).
[41] P. C. Engelking and W. C. Lineberger, Phys. Rev. A **19**, 149 (1979).
[42] E. Tiesinga, P. J. Mohr, D. B. Newell, and B. N. Taylor, 2018 NIST CODATA recommended values of the fundamental physical constants (NIST, Gaithersburg, MD), http://physics.nist.gov/constants (retrieved 2019).
[43] C. F. Fischer, M. Godefroid, T. Brage, P. Jönsson, and G. Gaigalas, J. Phys. B **49**, 182004 (2016).
[44] P. Jönsson, G. Gaigalas, J. Bieroń, C. F. Fischer, and I. P. Grant, Comput. Phys. Commun. **184**, 2197 (2013).
[45] L. Sturesson, P. Jönsson, and C. F. Fischer, Comput. Phys. Commun. **177**, 539 (2007).
[46] B. J. Mackenzie, I. P. Gran, and P. H. Norrington, Comput. Phys. Commun. **21**, 233 (1980).
[47] R. Si and C. F. Fischer, Phys. Rev. A **98**, 052504 (2018).
[48] D. Datta and D. R. Beck, Phys. Rev. A **50**, 1107 (1994).
[49] F. A. Babushkin Acta Phys. Pol. **25**, 749 (1964).
[50] P. Jönsson, X. He, C. F. Fischer, and I. P. Grant, Comput. Phys. Commun. **177**, 597 (2007).